

Exciton condensation driven by bound states of Green's functions zeros

Ivan Pasqua,¹ Andrea Blason,¹ and Michele Fabrizio¹

¹*International School for Advanced Studies (SISSA), Via Bonomea 265, I-34136 Trieste, Italy*

The interaction driven transition between quantum spin-Hall and Mott insulators in the Bernevig, Hughes and Zhang model is studied by dynamical cluster approximation, and found to be accompanied by the emergence of Green's function zeros already in the quantum spin-Hall regime. The non-trivial interplay between Green's function poles and zeros leads to an exotic quantum spin-Hall insulator exhibiting two chiral branches of edge Green's function poles and one of zeros. When symmetry breaking is allowed, a non-topological excitonic insulator is found to intrude between quantum spin-Hall and Mott insulators. We find evidence that excitons in the Mott insulator, which become soft at the transition to the excitonic insulator, are actually bound states between valence and conduction bands of Green's function zeros, rather than between lower and upper Hubbard bands.

INTRODUCTION

Upon increasing the electron-electron interaction strength, models of topological band insulators (TBIs) can be driven into supposedly-trivial, non-symmetry breaking correlated insulators (CIs) without the expected closing at the transition of the single-particle gap. Several ways have been found that allow circumventing the occurrence of a metal point between TBI and CI. The simplest and most direct is a discontinuous character of the transition [1, 2], but there seem to exist other more subtle routes connecting a TBI to a CI without crossing a metal.

For instance, a new insulating phase can intrude between TBI and CI that spontaneously breaks the symmetry which protects the topology. In the Bernevig, Hughes and Zhang (BHZ) model of quantum spin-Hall insulators (QSHIs) [3], this phase describes a magnetoelectric excitonic insulator, which thus breaks parity and time-reversal [4, 5]. As a matter of fact, exciton condensation is a logical outcome when the single-particle gap gets small around the TBI-CI transition. Indeed, there is evidence of indirect-exciton condensation in monolayer WTe₂ [6], which leads to a topological insulator that breaks time-reversal symmetry.

A further and rather exotic scenario is that the TBI-to-CI transition is direct and continuous, the single-particle gap remains finite and smooth, and, yet, a gapless point emerges within the particle-hole and/or particle-particle spectra. Slagle, You and Xu [7] have studied an AA-stacked honeycomb-lattice bilayer where each layer is described by a Kane-Mele model [8] of a QSHI plus an on-site Hubbard U , and the two layers are coupled to each other by an antiferromagnetic exchange J . Upon increasing U at large $J/U = 2$, they find a continuous transition from the QSHI to a trivial CI that is simply a collection of inter-layer singlets. At the transition, the single-particle gap remains finite whereas the spin gap as well as the gap to adding/removing two electrons vanish. This result raises an interesting issue. Indeed, the QSHI phase is characterised by a topological invariant $C_{\uparrow} = -C_{\downarrow} = \pm 1$, with C_{σ} the Chern number of the σ -band, which is also the winding number $W(G_{\uparrow}) = -W(G_{\downarrow})$ of the map

$(\epsilon, \mathbf{k}) \rightarrow G_{\uparrow}(i\epsilon, \mathbf{k}) \in GL(2, \mathbb{C})$ [9], where $G_{\uparrow}(i\epsilon, \mathbf{k})$ is the spin-up Green's function in Matsubara frequencies ϵ , and \mathbf{k} the two-dimensional momentum. Remarkably, the winding number retains the same quantised value on both sides of the transition [7], which, in turn, implies that the topological bands of poles of the QSHI Green's function determinant at real, negative frequencies transform into topological bands of zeros in the CI [7, 10–13]. We emphasise that the topological invariant $W(G_{\uparrow}) - W(G_{\downarrow})$ corresponds to the quantised spin-Hall conductance $C_{\uparrow} - C_{\downarrow}$ in the QSHI, but it does not in the CI [7, 12, 14].

How the transmutation of topological poles into topological zeros occurs across the transition is not known but in rather artificial cases [15]. It is also unclear whether such change of analyticity bears any signature of the vanishing spin and charge- $2e$ gaps, even though it is tempting to argue that their closing despite the finite charge- e gap corresponds to a Dirac-like touching of the bands of zeros, thus the emergence of a Luttinger surface [16], made just of two points in the specific case.

In this work we try to shed some light on those issues studying the transition in the BHZ model [3] between QSHI and CI, where the presence of the intermediate excitonic insulator (EI) phase raises further intriguing questions. Indeed, within dynamical mean-field theory (DMFT) [17] the transition upon increasing the interaction strength U between the EI and the Mott correlated insulator (MI) is continuous [5], which implies the existence of an excitonic mode in the Mott phase that gets soft approaching the transition and condenses beyond it, in the EI. In spite of that, the single-particle gap is sizeable and smooth across the transition [5]. In other words, the exciton softening seems to a large extent unrelated to the Mott gap between lower and upper Hubbard bands. Since the latter entail in-gap bands of zeros, it is tempting to argue that the excitons are bound states of valence and conduction bands of zeros, a suggestive conjecture that we shall investigate.

I. MODEL AND METHODS

We consider the BHZ model [3] for the QSHI phase of HgTe quantum wells. This model involves two spinful Wannier orbitals per unit cell, one that transforms like s -orbitals, $|\ell = 0, \sigma\rangle \equiv |s\sigma\rangle$, $\sigma = \uparrow, \downarrow$ being the spin projection along z , and the other like the $J = 3/2$, $J_z = \pm 3/2$ spin-orbit coupled combinations of p -orbitals, $|\ell = 1, \ell_z = +1, \uparrow\rangle \equiv |p\uparrow\rangle$ and $|\ell = 1, \ell_z = -1, \downarrow\rangle \equiv |p\downarrow\rangle$. We introduce two sets of Pauli matrices, σ_a and τ_a , $a = 0, \dots, 3$, with $a = 0$ denoting the identity, which act, respectively, in the spin, \uparrow and \downarrow , and orbital, s and p , spaces.

With those definitions, the BHZ tight-binding Hamiltonian on a square lattice and in momentum space reads

$$H_0 = \sum_{\mathbf{k}} \Psi_{\mathbf{k}}^\dagger \hat{H}_0(\mathbf{k}) \Psi_{\mathbf{k}}, \quad (1)$$

at density corresponding to two electrons per site, where $\Psi_{\mathbf{k}}^\dagger = (s_{\mathbf{k}\uparrow}^\dagger, s_{\mathbf{k}\downarrow}^\dagger, p_{\mathbf{k}\uparrow}^\dagger, p_{\mathbf{k}\downarrow}^\dagger)$ are four component spinors. In this representation, $\hat{H}_0(\mathbf{k})$ is the 4×4 matrix

$$\begin{aligned} \hat{H}_0(\mathbf{k}) = & \left(M - t(\cos k_x + \cos k_y) \right) \sigma_0 \otimes \tau_3 \\ & + \lambda \sin k_x \sigma_3 \otimes \tau_1 - \lambda \sin k_y \sigma_0 \otimes \tau_2. \end{aligned} \quad (2)$$

Hereafter, we set $t = 1$, the energy unit, $\lambda = 0.3$, half-filled density, i.e., two electrons per site, and, without loss of generality, $M \geq 0$.

For $M < 2$ the Hamiltonian (2) describes a QSHI, otherwise a conventional non-topological band insulator.

The periodic model (1) is invariant under C_4 , inversion \mathcal{I} , particle-hole \mathcal{P} and time-reversal \mathcal{T} symmetries, as well as under spin $U(1)$ rotations around the z -axis.

The on-site Coulomb interaction projected onto the Wannier orbital basis can be written as

$$H_{\text{int}} = \sum_{\mathbf{R}} H_{\text{int}}(\mathbf{R}), \quad (3)$$

where \mathbf{R} labels the lattice sites and

$$\begin{aligned} H_{\text{int}}(\mathbf{R}) = & U_s n_{s\mathbf{R}\uparrow} n_{s\mathbf{R}\downarrow} + U_p n_{p\mathbf{R}\uparrow} n_{p\mathbf{R}\downarrow} \\ & + V n_{s\mathbf{R}} n_{p\mathbf{R}} + H_{\text{dip}}(\mathbf{R}), \end{aligned} \quad (4)$$

with $n_{a\mathbf{R}\sigma}$ the number of spin $\sigma = \uparrow, \downarrow$ electrons at site \mathbf{R} in orbital $a = s, p$, and $n_{a\mathbf{R}} = n_{a\mathbf{R}\uparrow} + n_{a\mathbf{R}\downarrow}$. The term $H_{\text{dip}}(\mathbf{R})$ in (4) is the dipole component of the multipole expansion of the Coulomb interaction,

$$\begin{aligned} H_{\text{dip}}(\mathbf{R}) = & \frac{J}{2} \left\{ \left(\Psi_{\mathbf{R}}^\dagger \sigma_0 \otimes \tau_1 \Psi_{\mathbf{R}} \right)^2 \right. \\ & \left. + \left(\Psi_{\mathbf{R}}^\dagger \sigma_3 \otimes \tau_2 \Psi_{\mathbf{R}} \right)^2 \right\} \\ = & J \left(s_{\mathbf{R}\uparrow}^\dagger s_{\mathbf{R}\downarrow}^\dagger p_{\mathbf{R}\downarrow} p_{\mathbf{R}\uparrow} + p_{\mathbf{R}\uparrow}^\dagger p_{\mathbf{R}\downarrow}^\dagger s_{\mathbf{R}\downarrow} s_{\mathbf{R}\uparrow} \right. \\ & \left. + s_{\mathbf{R}\uparrow}^\dagger p_{\mathbf{R}\uparrow}^\dagger s_{\mathbf{R}\uparrow} p_{\mathbf{R}\uparrow} + s_{\mathbf{R}\downarrow}^\dagger p_{\mathbf{R}\downarrow}^\dagger s_{\mathbf{R}\downarrow} p_{\mathbf{R}\downarrow} \right), \end{aligned} \quad (5)$$

where $\Psi_{\mathbf{R}}$ is the Fourier transform in real space of the spinor $\Psi_{\mathbf{k}}$, \mathbf{R} being a lattice site. All parameters, U_s , U_p , V and J are positive. The interaction (4) enforces Hund's rules when $\min(U_s, U_p) > V$, which we assume hereafter and entails that the lowest energy two-electron configuration of $H_{\text{int}}(\mathbf{R})$ is a spin triplet, $S = 1$, with $S_z = \pm 1$.

However, for completeness, we will also consider the case $J < 0$. This may occur when the electrons are strongly coupled to an infrared optical mode twofold degenerate by C_4 ,

$$\begin{aligned} H_{\text{el-ph}}(\mathbf{R}) = & q_{1\mathbf{R}} \left(\Psi_{\mathbf{R}}^\dagger \sigma_0 \otimes \tau_1 \Psi_{\mathbf{R}} \right) \\ & + q_{2\mathbf{R}} \left(\Psi_{\mathbf{R}}^\dagger \sigma_3 \otimes \tau_2 \Psi_{\mathbf{R}} \right), \end{aligned}$$

which, integrating out phonons and discarding retardation effects, yields an effective interaction of the same form as (5) but with a negative coupling constant. When the latter overwhelms the Coulomb exchange, the net effect is a dipole term (5) with an effective $J < 0$. In this case, the ground state of $H_{\text{int}}(\mathbf{R})$ with two electrons is twofold degenerate and comprises the states where the two orbitals are singly occupied and coupled either in a spin-singlet, $S = 0$, or in a spin-triplet, $S = 1$, with $S_z = 0$.

To make contact with [7], we will add for $J < 0$ the additional term

$$\delta H_{\text{dip}}(\mathbf{R}) = -\delta J \left(s_{\mathbf{R}\uparrow}^\dagger p_{\mathbf{R}\downarrow}^\dagger s_{\mathbf{R}\downarrow} p_{\mathbf{R}\uparrow} + H.c. \right), \quad (6)$$

with $\delta J > 0$, which lowers the energy of the singlet configuration and thus stabilises a non-magnetic Mott insulator, actually a Van Vleck paramagnet because spin $SU(2)$ is broken. We remark, however, that (6) breaks explicitly the C_4 symmetry, $p_{\mathbf{R}\uparrow} \rightarrow i p_{\mathbf{R}\uparrow}$ and $p_{\mathbf{R}\downarrow} \rightarrow -i p_{\mathbf{R}\downarrow}$.

A. Leading symmetry breaking channels

The leading symmetry breaking channels can be identified as the most negative bare scattering amplitudes [4]. To reduce the parameter freedom and thus simplify the analysis, we hereafter take $U_s = U_p = U$. We define the local scattering channels and the corresponding bare scattering amplitudes as $\Psi_{\mathbf{R}}^\dagger \sigma_a \otimes \tau_b \Psi_{\mathbf{R}}$ and Γ_{ab}^0 , respectively.

For $J > 0$, the most negative symmetry breaking amplitudes are [4]

- $\Gamma_{30}^0 = -(U+2J)/4$, which tends to stabilise ferro or antiferro magnetic order with local magnetisation parallel or antiparallel to z ;
- $\Gamma_{11}^0 = \Gamma_{21}^0 = -(V+2J)/4$, degenerate by spin $U(1)$, which can drive an exciton condensation with order parameter

$$\begin{aligned} \Delta(\phi) = & \cos \phi \langle \Psi_{\mathbf{R}}^\dagger \sigma_1 \otimes \tau_1 \Psi_{\mathbf{R}} \rangle \\ & + \sin \phi \langle \Psi_{\mathbf{R}}^\dagger \sigma_2 \otimes \tau_1 \Psi_{\mathbf{R}} \rangle, \end{aligned} \quad (7)$$

breaking \mathcal{I} , \mathcal{T} and spin $U(1)$ symmetries.

Since $U > V$, the magnetic instability is more likely in the MI. However, as we mentioned, the excitonic instability does emerge between the QSHI and MI.

For $J < 0$, the most negative symmetry breaking amplitudes are instead [4]

- $\Gamma_{33}^0 = -(U + 2|J|)/4$, which favours an ordering in the Mott phase of the local configurations $s_{\mathbf{R}\uparrow}^\dagger p_{\mathbf{R}\downarrow}^\dagger$ and $p_{\mathbf{R}\uparrow}^\dagger s_{\mathbf{R}\downarrow}^\dagger$;
- $\Gamma_{01}^0 = \Gamma_{32}^0 = -(V + 4|J|)/4$, degenerate by C_4 , which can drive an exciton condensation.

Adding a weak $\delta J > 0$, which we recall breaks C_4 , stabilises a non-magnetic Mott insulator where each site is locked into the inter-orbital spin-singlet

$$\frac{1}{\sqrt{2}} \left(s_{\mathbf{R}\uparrow}^\dagger p_{\mathbf{R}\downarrow}^\dagger + p_{\mathbf{R}\uparrow}^\dagger s_{\mathbf{R}\downarrow}^\dagger \right) |0\rangle,$$

whereas the leading excitonic instability corresponds to the order parameter

$$\Delta = \langle \Psi_{\mathbf{R}}^\dagger \sigma_0 \otimes \tau_1 \Psi_{\mathbf{R}} \rangle, \quad (8)$$

that breaks inversion.

B. Methods

The results that we present hereafter are obtained by the so-called dynamical cluster approximation (DCA) [18], which consists in partitioning the Brillouin zone into patches and in approximating the self-energy as a piecewise constant function within these patches. The many-body problem is tackled by self-consistently solving coupled quantum impurity models. The impurity solver is implemented within the TRIQS library [19] and makes use of a continuous time quantum Monte Carlo algorithm based on a hybridization expansion of the partition function [20, 21].

In order to reconstruct a smooth momentum dependence from the piecewise constant self-energy obtained in DCA, one can follow two alternative routes: either periodise the self-energy or its inverse in terms of hopping processes with increasing spatial range, consistently with the space group symmetry and the finite number of patches. The former approximation seems to work better at weak coupling, while the latter, known as cumulant periodisation [22], is more suitable when the self-energy develops singularities in the Brillouin zone, which commonly occurs near the Mott transition and inside the Mott insulator. In the calculations we employ just two patches centred around $\mathbf{\Gamma} = (0, 0)$ and $\mathbf{M} = (\pi, \pi)$, which was already computationally expensive since the model has two interacting orbitals per site. We use the same partition of the Brillouin zone as in [23], in which the patch at \mathbf{M} includes also the $\mathbf{X} = (\pi, 0)$ and $\mathbf{Y} = (0, \pi)$ points, but

we checked that different partitions do not change appreciably the results.

The 2-patch scheme has however a drawback that it is worth highlighting now. The Green's function $\hat{G}(i\epsilon, \mathbf{k})$ in Matsubara frequencies $\epsilon = (2\ell + 1)\pi T$ with $\ell \in \mathbb{Z}$, is a 2×2 matrix satisfying Dyson's equation

$$\hat{G}(i\epsilon, \mathbf{k})^{-1} = i\epsilon - \hat{H}_0(\mathbf{k}) - \hat{\Sigma}(i\epsilon, \mathbf{k}), \quad (9)$$

where the self-energy matrix $\hat{\Sigma}(i\epsilon, \mathbf{k})$ encodes all interaction effects. However, $\hat{\Sigma}(i\epsilon, \mathbf{k})$ is purely diagonal at $\mathbf{k} = \mathbf{\Gamma}, \mathbf{M}$ because of inversion symmetry. Therefore, by using just the two patches at $\mathbf{\Gamma}$ and \mathbf{M} , we cannot access the off-diagonal elements of $\hat{\Sigma}(i\epsilon, \mathbf{k})$ that must exist away from the inversion symmetry points, and which would require a number of patches ≥ 8 that is numerically intractable for us. In the following, we shall point out features of our results that may be critically affected by this limitation, and argue what could change should we use a larger number of patches.

Finally, before delving into the analysis of our results, let us recall a recently introduced interpreting scheme [16] aimed at providing a quasiparticle description applicable to both weakly and strongly correlated regimes. We write the interacting Green's function matrix on the Matsubara frequency axis as

$$\begin{aligned} \hat{G}(i\epsilon, \mathbf{k}) &= \frac{1}{i\epsilon - \hat{H}_0(\mathbf{k}) - \hat{\Sigma}(i\epsilon, \mathbf{k})} \\ &= \hat{A}(\epsilon, \mathbf{k}) \frac{1}{i\epsilon - \hat{H}_*(\mathbf{k})} \hat{A}(\epsilon, \mathbf{k})^\dagger \\ &\equiv \hat{A}(\epsilon, \mathbf{k}) G_*(i\epsilon, \mathbf{k}) \hat{A}(\epsilon, \mathbf{k})^\dagger, \end{aligned} \quad (10)$$

where, if we define the hermitian matrices

$$\begin{aligned} \hat{\Sigma}_1(i\epsilon, \mathbf{k}) &= \frac{\hat{\Sigma}(i\epsilon, \mathbf{k}) + \hat{\Sigma}(i\epsilon, \mathbf{k})^\dagger}{2}, \\ \hat{\Sigma}_2(i\epsilon, \mathbf{k}) &= \frac{\hat{\Sigma}(i\epsilon, \mathbf{k}) - \hat{\Sigma}(i\epsilon, \mathbf{k})^\dagger}{2i}, \end{aligned} \quad (11)$$

since $\hat{\Sigma}(i\epsilon, \mathbf{k})^\dagger = \hat{\Sigma}(-i\epsilon, \mathbf{k})$, then

$$\begin{aligned} \hat{Z}(\epsilon, \mathbf{k}) &= \hat{Z}(-\epsilon, \mathbf{k}) = \left(1 - \frac{\hat{\Sigma}_2(i\epsilon, \mathbf{k})}{\epsilon} \right)^{-1} \\ &= \hat{A}(\epsilon, \mathbf{k})^\dagger \hat{A}(\epsilon, \mathbf{k}), \end{aligned} \quad (12)$$

is a semi positive-definite matrix, while the hermitian *quasiparticle* (QP) Hamiltonian reads

$$\begin{aligned} \hat{H}_*(\epsilon, \mathbf{k}) &= \hat{H}_*(-\epsilon, \mathbf{k}) \\ &= \hat{A}(\epsilon, \mathbf{k}) \left(\hat{H}_0(\mathbf{k}) + \hat{\Sigma}_1(i\epsilon, \mathbf{k}) \right) \hat{A}(\epsilon, \mathbf{k})^\dagger. \end{aligned} \quad (13)$$

In our discussion we will always refer to the low-energy behaviour of the QP Hamiltonian $\hat{H}_*(0, \mathbf{k}) = \hat{H}_*(\mathbf{k})$. In the weakly interacting QSHI regime the QP bands practically coincide with the dispersive poles of the Green's

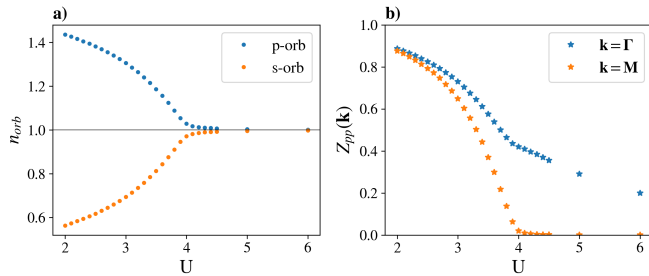


FIG. 1. Panel a): Renormalization of the occupations in the two orbitals across the QSHI-MI transition, at fixed $M = 0.9$. Deep in the MI phase $n_p - n_s$ decays as $1/U^3$. Panel b): Quasiparticle residue $\hat{Z}_{pp}(\mathbf{k}) = \hat{Z}_{ss}(\mathbf{k})$ computed from the imaginary part of the self-energy at the first Matsubara frequency. In the \mathbf{M} -patch it is strongly suppressed inside the MI, signaling the proximity to a self-energy pole. The change of concavity around $U \sim 4$ is identified as the onset of Mottness.

function. In the MI instead, the in-gap QP bands are related to the presence of in-gap bands of Green's function zeros on the real axis, i.e., to the roots of

$$\det(G(i\epsilon \rightarrow \epsilon_{\mathbf{k}}, \mathbf{k})) = 0, \quad \epsilon_{\mathbf{k}} \in \mathbb{R}.$$

The QP bands and $-\epsilon_{\mathbf{k}}$ coincide in the limit of very large Mott-Hubbard gap [12, 13]. We will show that such a correspondence is effective even for intermediate coupling, thus facilitating a description of the excitonic instability.

II. THE SYMMETRIC QSHI-MI TRANSITION

Unless stated otherwise, the numerical results were obtained at $\beta = 50$ and it was checked their stability upon decreasing the temperature.

A. The $J > 0$ case

We set $V = U - 2J$ and $J = U/4$. The phase diagram in the (U, M) plane within the DMFT approximation has been extensively discussed with and without excitonic symmetry breaking [5]. First of all, we here address the symmetric QSHI to MI transition, i.e. in absence of spontaneous symmetry breaking (SSB). In single-site DMFT the transition is first order, but we will argue that the inclusion of non-local correlations using the DCA scheme changes the picture. In Fig. 1 we show the occupation number n_{orb} in the two orbitals as we increase the interaction strength U at fixed $M = 0.9$. For weak interaction strength the model is a QSHI adiabatically connected to the non-interacting one and the main contribution of the interaction is a renormalization of the on-site mass difference between the two orbitals and, consequently, of the

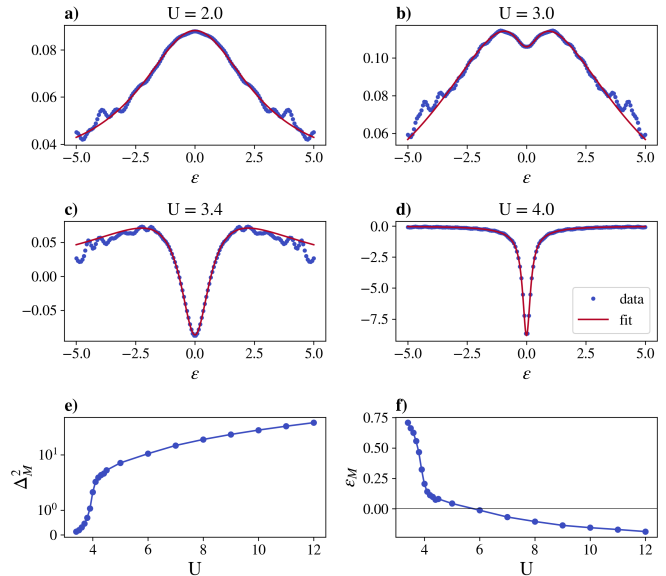


FIG. 2. Panels a, b, c, d): $\Delta \hat{\Sigma}_{pp}(i\epsilon, \mathbf{M}) = -\hat{\Delta} \Sigma_{ss}(i\epsilon, \mathbf{M})$ for 4 different values of U , at fixed $M = 0.9$. For $U \geq 3$ a narrower peak appears and becomes dominant as we increase the interaction strength. There is a good agreement between the data and the fit (15), from which we can extract information about the narrower Lorentzian. Panels e, f): fit parameters of the narrower Lorentzian related with a pole-like structure emerging in the self-energy. ϵ_M changes sign between $U = 5$ and $U = 6$ through a Luttinger Dirac-like surface in \mathbf{M} .

orbital magnetization $n_p - n_s$:

$$M_{\text{eff}} = M + \frac{1}{4} \text{Tr}[\sigma_0 \otimes \tau_3 \hat{\Sigma}(i\epsilon = 0)] \quad (14)$$

where $\hat{\Sigma}(i\epsilon) = (\hat{\Sigma}(i\epsilon, \mathbf{\Gamma}) + \hat{\Sigma}(i\epsilon, \mathbf{M}))/2$ is the local self-energy. In the strong coupling regime the system is a MI with almost identical occupation in the two orbitals. Indeed, deep in the Mott insulating phase, one expects in perturbation theory that $n_p - n_s$ decays as $1/U^3$. Since $J > 0$ enforces Hund's rules, the two electrons localised on each site form a spin triplet state with $S_z = \pm 1$, thus the acronym hs-MI where hs stands for high-spin. For completeness in Fig. 1 we show also the quasiparticle residue (12) in the two patches computed from the imaginary part of the self-energy at the first Matsubara frequency $i\epsilon_1 = i\pi T$. Differently from the DMFT case, we observe no first order discontinuity in the quantities discussed above, which makes harder to localize the transition to the MI, since the orbitals are truly at half-filling only for $U \rightarrow \infty$. Nevertheless, around $U \sim 4$ we observe a change of concavity in the plotted quantities, which we can identify as the onset of the MI.

In Fig. 2 we plot $\Delta \hat{\Sigma}_{pp}(i\epsilon, \mathbf{k}) = \text{Re} \hat{\Sigma}_{pp}(i\epsilon, \mathbf{k}) - \hat{\Sigma}_{pp}^{\text{HF}}$ as a function of ϵ for different values of U , where $\hat{\Sigma}_{pp}^{\text{HF}}$ is the Hartee-Fock contribution, i.e. the $|\epsilon| \rightarrow \infty$ limit of the self-energy. We observe that $\Delta \hat{\Sigma}_{pp}(i\epsilon, \mathbf{M}) =$

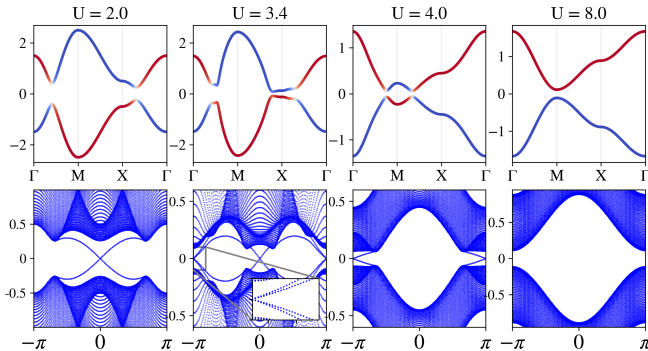


FIG. 3. Using the parameters fitted from the self-energy (see Fig. 2) in the toy model (16) we computed the bands of $\hat{H}_*(0, \mathbf{k})$ for 4 different values of U , both in PBC (upper panels) and OBC (lower panels). The colours of the lines represent the orbital character of the eigenvectors, blue (red) for the s-(p)-character. For $U = 2.0$ the system is adiabatically connected to the non-interacting QSHI. For $U = 3.4$ the topology is unchanged, but in OBC we recognize three pairs of chiral edge states: two associated with Green's function poles and one with zeros. In the inset we zoomed a region around $\mathbf{k} = -\pi$. For $U = 4$ the model turns into a MI that has topological in-gap bands of zeros with winding numbers opposite to the QSHI. Finally for $U = 8$ the in-gap zeros are topologically trivial and smoothly connected to the atomic limit.

$-\hat{\Delta}\Sigma_{ss}(i\epsilon, \mathbf{M})$ looks like the difference of a very broad Lorentzian-like function and a narrower one that appears above $U = 3$ and grows with further increase of U , while it is the sum of two Lorentzians if we look at the patch Γ . Therefore, we fit the frequency dependence with two Lorentzian functions

$$\Delta\hat{\Sigma}_{pp}(i\epsilon, \mathbf{k}) = -\frac{\alpha_{\mathbf{k}} \gamma_{\mathbf{k}}^2}{\epsilon^2 + \alpha_{\mathbf{k}}^2} - \frac{\epsilon_{\mathbf{k}} \Delta_{\mathbf{k}}^2}{\epsilon^2 + \epsilon_{\mathbf{k}}^2} \quad (15)$$

where the first Lorentzian is smooth, broad and qualitatively the same in the two patches while the second one is narrower and opposite in sign in the two patches. We associate the latter with the emergence of a pole-like structure in the self-energy that becomes dominant in the MI phase. Looking at the fit parameters of the latter we can identify two trends: first, $\Delta_{\mathbf{M}}^2$ increases making the contribution due to this Lorentzian dominant in the MI; second, $\epsilon_{\mathbf{M}}$ changes sign between $U = 5$ and $U = 6$. To rationalize such a behaviour we consider a toy model where the effect of the broader Lorentzian is captured in a renormalization of the effective on-site mass M and for the frequency dependent part of the self-energy we retain only the singular Lorentzian. Then the renormalized energies are given by

$$\hat{R}(\mathbf{k}) = \hat{H}_0(\mathbf{k}) + \hat{\Sigma}_1(0, \mathbf{k}) = \hat{H}_0(\mathbf{k}) + \frac{\Delta^2}{\hat{H}_1(\mathbf{k})}, \quad (16)$$

where $\hat{H}_0(\mathbf{k})$ has an effective mass $M_{\text{eff}} < M$, and $\hat{H}_1(\mathbf{k})$ resembles $\hat{H}_0(\mathbf{k})$ in (2) though with renormalized pa-

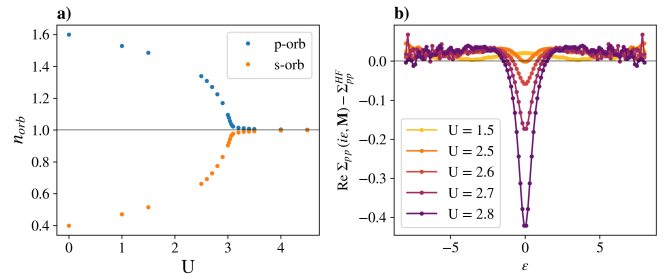


FIG. 4. Panel a): Renormalization of the occupations in the two orbitals across the QSHI-MI transition, at fixed $M = 1.0$ and $J < 0$. Panel b): $\Delta\hat{\Sigma}_{pp}(i\epsilon, \mathbf{M}) = -\hat{\Delta}\Sigma_{ss}(i\epsilon, \mathbf{M})$ for some values of U before the onset of Mottness ($U \sim 3.1$). The phenomenology is the same already discussed in the $J > 0$ case, as we can conclude comparing with Fig. 1 and Fig. 2.

rameters. The change of sign of $\epsilon_{\mathbf{M}}$ corresponds to a change of the mass M_1 in $\hat{H}_1(\mathbf{k})$ from $-2t_1 < M_1 < 0$ to $M_1 < -2t_1$, i.e. a topological phase transition of the dispersive poles of the self-energy through a Dirac-like Luttinger surface, actually a point at \mathbf{M} . Finally, we recall that we do not have direct access to the off-diagonal elements of $\Sigma(i\epsilon, \mathbf{k})$ which will be non-zero away from the high-symmetry points. It has been shown [24] that such terms do not play a crucial role in the QSHI-MI transition. Nonetheless, in the following discussion we add to $\hat{H}_1(\mathbf{k})$ in (16) a small $\lambda_1 = 0.2$ to correctly reproduce the gapping of the Luttinger surfaces away from the high-symmetry points.

In Fig. 3, we plot the bands of the QP Hamiltonian $\hat{H}_*(\mathbf{k}) = \hat{H}_*(0, \mathbf{k})$, see (13), both in periodic boundary conditions (PBC) and in open boundary conditions (OBC) along one direction [25]. For small values of the interaction (first panel) there is only a renormalization of the on-site mass difference, thus the system is adiabatically connected to the non-interacting QSHI and, in OBC, it has in-gap genuine chiral edge states, i.e., gapless surface Green's function poles. Increasing the interaction strength (second panel), dispersive poles appear in the self-energy ($\Delta \neq 0$), i.e., Green's function zeros, but, at first, without passing through a bulk gapless point, thus leaving unchanged the topological invariant. We observe that in OBC there are actually three pairs of chiral edge states: two associated with Green's function poles and one with zeros. This phase, in which there is a non-trivial interplay between the topological band of poles and zeros, has been recently observed [26] in a model topological Kondo insulator and dubbed *topological pseudogap insulator*. Upon further increasing U (third panel), the system undergoes a topological phase transition: the gap between the bands of poles closes at the high-symmetry points \mathbf{X} and \mathbf{Y} . Beyond this semi-metal point, the model turns into a MI that has topological in-gap bands of zeros with winding numbers $W(G_\sigma)$ opposite to the QSHI, and not necessarily corresponding to finite Chern numbers C_σ [12]. In OBC we find only a

pair of chiral edge zeros. Finally, deep inside the MI also the zeros become topologically trivial and the system can smoothly evolve towards the atomic limit (fourth panel). Finally, we want to emphasize that the continuous nature of the QSHI-MI transition remains robust even lowering the temperature, indicating that this is not merely a finite temperature effect but more likely the consequence of the appearance of Green's function bands of zeros already in the QSHI, which smoothly evolve in the MI upon increasing U .

B. The $J < 0$ case

We now briefly discuss the symmetric QSHI-MI phase transition in the $J < 0$ case. We choose $J = -\frac{U}{2}$ so that $V = 0$, which allows us to make a direct comparison with the bilayer model investigated in [7] where the two layers interact solely via an antiferromagnetic exchange. As previously discussed, we also add the interaction term (6) to favour the on-site spin-singlet configuration, thus a low-spin MI (ls-MI). In our computation, we set $\delta J = U/16$.

In Fig. 4 we show the occupation numbers n_{orb} of the two orbitals with increasing U at fixed $M = 1.0$, as well as $\Delta\hat{\Sigma}_{pp}(i\epsilon, \mathbf{k}) = \text{Re}\hat{\Sigma}_{pp}(i\epsilon, \mathbf{k}) - \hat{\Sigma}_{pp}^{\text{HF}}$ as a function of ϵ for different values of U . We find that the phenomenology of the QSHI-MI phase transition in this case is the same as for positive J , thus occurs through a closing of the single-particle gap. This is different from what was reported in [7], where a similar but different model was examined. Additionally, in their study, they set $|J|/U = 2$, meaning the transition is controlled by the J term, whereas in our study the transition is driven by U .

III. THE EXCITONIC INSTABILITY

A. The $J > 0$ case

We now investigate what could happen if we allow for spontaneous symmetry breaking (SSB) in the system. In particular, we focus on the possible emergence of an exciton condensate characterized by the order parameter (7), e.g., at $\phi = 0$,

$$P_1 = \langle \Psi_{\mathbf{R}}^\dagger \sigma_1 \otimes \tau_1 \Psi_{\mathbf{R}} \rangle. \quad (17)$$

We call excitonic insulator (EI) the phase where $P_1 \neq 0$, which breaks the symmetries that protect the non-trivial topology of the QSHI. In Fig. 5 we plot P_1 as a function of the interaction strength for different values of M . Both the QSHI-EI and EI-MI transitions seem to be second order within 2-patches DCA. We recall that in single site DMFT at $T = 0$ only the latter is so, while the QSHI-EI one is first order [5]. For smaller values of M , the range of stability of the EI shrinks. This could already be observed in DMFT, though the EI survives down to

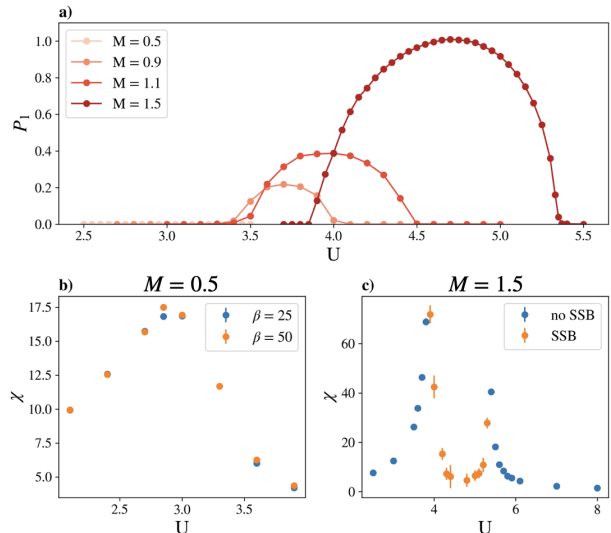


FIG. 5. Panel a): Excitonic order parameter P_1 as a function of the interaction strength U for 4 different values of M . As we decrease M the bell-like dependence is strongly renormalized both in height and width, until for $M = 0.5$ no condensation appears. The results we show are stable until the lowest temperature we checked, i.e. $\beta = 150$. Panel b): We support the claim that for small values of M (e.g. $M = 0.5$) no condensation appears with the computation of the susceptibility χ to an external field coupled to the excitonic order parameter. There is no substantial difference between $\beta = 25$ and $\beta = 50$, further suggesting this is not a temperature consequence. Panel c): For $M = 1.5$ the susceptibility diverges at the phase boundaries of the EI.

$M \rightarrow 0$. On the contrary, the non-local correlations captured in DCA seem to prevent the stabilisation of such a phase for $M \lesssim 0.6$, at least down to the lowest accessible temperatures. This scenario is further supported by the direct computation at $M = 0.5$ of the static and uniform susceptibility χ to a field coupled to the excitonic order parameter, see Fig. 5. In contrast to what we observe at larger M , e.g. $M = 1.5$, there is no value of U such that the susceptibility diverges. However, we cannot exclude that, at lower values of temperatures than those we can access, the EI does appear.

B. The $J < 0$ case

In this case the EI phase is characterized by an excitonic order parameter (8),

$$P_2 = \langle \Psi_{\mathbf{R}}^\dagger \sigma_0 \otimes \tau_1 \Psi_{\mathbf{R}} \rangle, \quad (18)$$

breaking \mathcal{I} , but not \mathcal{T} , see Fig. 6. However, unlike for $J > 0$, the QSHI-EI transition looks first order, while, the EI-MI transition is again second order. We notice that also with negative J , we cannot stabilize an EI at small values of M , at least down to the lowest numerically accessible temperature.

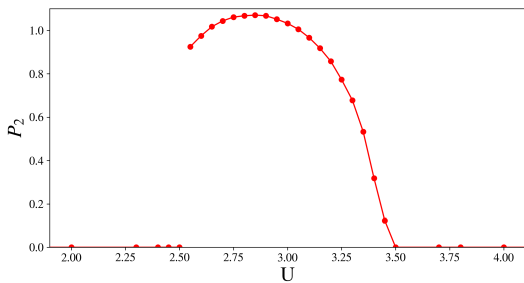


FIG. 6. Excitonic order parameter P_2 in the $J < 0$ case for $M = 1.0$. Differently from the $J > 0$ case the QSHI-to-EI transition is first order, while the EI-to-MI is still second order.

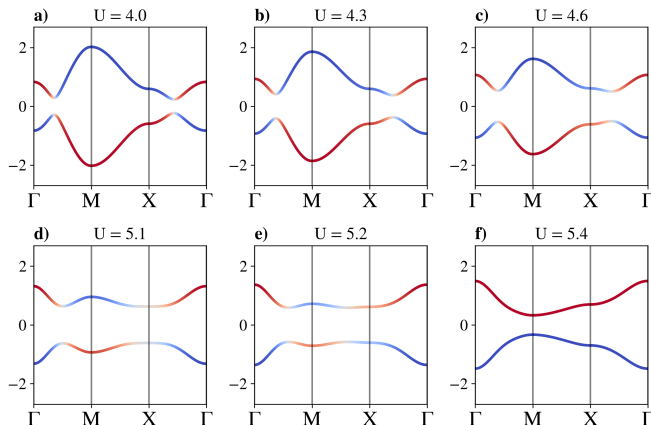


FIG. 7. Smooth evolution of the QP bands across the QSHI-EI-MI transitions. The colours of the lines represent the orbital character of the eigenvectors, blue(red) for the s-(p)-character. In panel a) the system is a QSHI. In panels b), c), d) and e) the system is an EI with $P_1 \neq 0$. The EI breaks inversion symmetry, indeed the orbital character at the high-symmetry points is no more well defined. In panel f) the QP bands closely resemble the dispersive Green's function zeros of a MI.

C. Excitonic instability of the Mott insulator and the quasiparticle scenario

Here, we try to shed some light on another intriguing issue related to the MI-EI transition, focusing for simplicity on the $J > 0$ case. Indeed, while the QSHI-EI transition can be conceptually grasped through the softening of an exciton bound state between valence and conduction bands as the single-particle gap shrinks upon increasing U , this picture is not justifiable at the MI-EI transition. In the MI, the single-particle gap typically remains large, seemingly precluding the formation of excitonic bound states capable of softening upon approaching the transition. This quite natural observation prompted us to explore whether in the MI the excitons can be regarded as bound states of the valence and conduction bands of Green's function zeros. The idea comes sponta-

neously once we notice that a Luttinger surface may host Landau's quasiparticles, similarly to a Fermi surface [27]. These quasiparticles cannot transport charge if the system is a true Mott insulator, but they are not neutral in the strict sense. In other words, one should imagine [28] that the quasiparticle motion in the MI is cancelled by a charge backflow so that there is no net longitudinal current flowing in an electric field. On the contrary, such dressed quasiparticle could still transport entropy, spin, and even experience a Lorentz force in a magnetic field [16, 26]. In our case, the quasiparticle carries an additional quantum number, the parity, which not only makes it possible the opening of a hybridisation gap, but also the existence of bound states between opposite-parity quasiparticle and quasihole excitations. Since these anomalous quasiparticles are closely related to in-gap bands of Green's functions zeros [12, 13, 29], we can indeed look upon their bound states as those between valence and conduction bands of Green's functions zeros. Interestingly enough, it has been shown in a similar model that a MI with a Luttinger surface has an odd-parity exciton susceptibility that is power-law in temperature, suggestive of the existence of gapless opposite-parity quasiparticles [26].

Moving back to our results, in Fig. 7 we show the QP bands across the two transitions for $M = 1.5$ and $J > 0$. In the following we will refer to U_{c1} (U_{c2}) the value correspondent to the QSHI-EI (EI-MI) transition. For $U < U_{c1} \simeq 3.9$, the system is a QSHI. For $U \in [U_{c1}, U_{c2}]$, with $U_{c2} \simeq 5.3$, we instead find the EI with $P_1 \neq 0$. As we mentioned, $P_1 \neq 0$ breaks inversion and, indeed, the orbital character at the high-symmetry points is no more well defined, see Fig. 7. Finally, for $U > U_{c2}$ the QP bands closely resemble the dispersive Green's function zeros of a MI. We observe that the QP bands evolve smoothly across the two very different transitions, which is a advantageous feature of the quasiparticle description outlined in the equations (10)-(13).

In Fig. 8 we show the QP gap, i.e., the gap of the QP Hamiltonian $H_*(\mathbf{k})$, versus the single-particle one extracted from the density-of-states (DOS). We emphasise that, in conventional insulators, the condensation of excitons is expected to raise the single-particle gap, since it generates an additional level repulsion between valence and conduction bands. This is indeed the case at the QSHI-EI transition, but in no way it occurs at the MI-EI transition, where the single-particle gap actually decreases, see Fig. 8. On the contrary, the QP gap does precisely what is expected: it grows entering the EI phase from both the QSHI and MI sides. We believe that this remarkable behaviour is a strong indication that the exciton that becomes soft in the MI is formed between valence and conduction bands of zeros rather than from the lower and upper Hubbard bands. This is further supported by the evidence that the single-particle gap in the MI is sizeable, which makes not conceivable that lower and upper Hubbard bands might be involved in the exciton softening. We end noticing that single-particle and

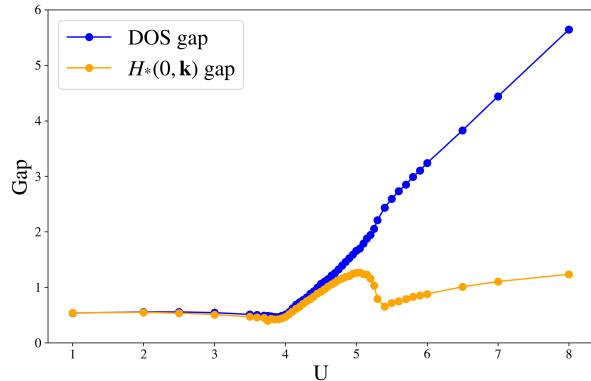


FIG. 8. Panel a): Comparison between the QP gap of $H_*(0, \mathbf{k})$ versus the single-particle one extracted from the DOS in the QSHI-EI-MI transitions. The point at which the two start to deviate signal that the bands of zeros come into play. We notice that in the MI phase the QP gap is much smaller than the DOS one and, as expected the condensation of excitons increases the QP gap due to the additional level repulsion between valence and conduction bands.

QP gaps are practically the same on increasing U up to around the value at which P_1 reaches a maximum, see Fig. 5. Above that, while the single-particle gap keeps growing with U , the QP one first decreases up to the Mott transition and then it raises again, though remaining much smaller than the single-particle gap. The point at which the two gaps start to deviate from each other is also that when the bands of zeros come into play, which thus occurs already in the EI. Indeed, looking at the low-frequency behavior of the self-energy in the EI we can still identify a structure made up of two Lorentzians, as the one we discussed in Fig. 2.

IV. CONCLUSIONS

We have extensively analysed the interacting BHZ model by means of dynamical cluster approximation [18], which allows us to study in detail the intriguing interplay between the bands of Green's function poles and those of

Green's function zeros upon approaching the Mott transition [10, 11]. We have discovered that bands of Green's function zeros emerge already in the quantum spin-Hall insulator, leading to a rather remarkable topological insulator exhibiting two chiral branches of edge Green's function poles and one of zeros, in that way leaving invariant the spin Chern number of the weakly correlated state [26] and thus without requiring a topological transition.

The Mott transition forcing symmetries occurs as usual through a semi-metal point where the single-particle gap closes at the high-symmetry \mathbf{X} and \mathbf{Y} points, though with a vanishing quasiparticle residue that entails a jump of the single-particle gap to the large separation between lower and upper Hubbard bands. However, inside the Mott insulator valence and conduction topological bands of Green's function zeros survive and induce, in open boundary conditions, edge zeros. At a critical value of the interaction strength the bands of zeros touch in a Dirac-like manner at the high-symmetry point \mathbf{M} , and, above such value, these bands become trivial and the Mott insulator is able to evolve smoothly into its atomic limit [13].

When we allow for symmetry breaking, a non-topological excitonic insulator is found to intrude between the quantum spin-Hall and Mott insulators [4, 5]. We do not find the expected magnetic instability in the Mott insulator, due to a well known flaw of the two-patch dynamical cluster approximation calculation [30] that we can afford. However, to ensure that our results are not an artifact of the approximation, we have also studied a model with an inverted exchange that stabilises a Van Vleck paramagnetic Mott insulator. Indeed, the two models show a similar behavior. In particular, we find evidence that the exciton in the Mott insulator, which becomes soft at the transition into the excitonic insulator, might actually be a bound state between valence and conduction bands of Green's function zeros rather than between lower and upper Hubbard bands, which are very distant in energy.

ACKNOWLEDGMENTS

We are very grateful to Adriano Amaricci and Carlos Mejuto Zaera for helpful discussions and comments.

-
- [1] A. Amaricci, J. C. Budich, M. Capone, B. Trauzettel, and G. Sangiovanni, Phys. Rev. Lett. **114**, 185701 (2015).
 - [2] A. Amaricci, J. C. Budich, M. Capone, B. Trauzettel, and G. Sangiovanni, Phys. Rev. B **93**, 235112 (2016).
 - [3] B. A. Bernevig, T. L. Hughes, and S.-C. Zhang, Science **314**, 1757 (2006).
 - [4] A. Blason and M. Fabrizio, Phys. Rev. B **102**, 035146 (2020).
 - [5] A. Amaricci, G. Mazza, M. Capone, and M. Fabrizio, Phys. Rev. B **107**, 115117 (2023).
 - [6] Y. Jia, P. Wang, C.-L. Chiu, Z. Song, G. Yu, B. Jäck, S. Lei, S. Klemenz, F. A. Cevallos, M. Onyszczyk, N. Fishchenko, X. Liu, G. Farahi, F. Xie, Y. Xu, K. Watanabe, T. Taniguchi, B. A. Bernevig, R. J. Cava, L. M. Schoop, A. Yazdani, and S. Wu, Nature Physics **18**, 87 (2022).
 - [7] K. Slagle, Y.-Z. You, and C. Xu, Phys. Rev. B **91**, 115121 (2015).
 - [8] C. L. Kane and E. J. Mele, Phys. Rev. Lett. **95**, 226801 (2005).

- [9] Z. Wang and S.-C. Zhang, *Phys. Rev. X* **2**, 031008 (2012).
- [10] V. Gurarie, *Phys. Rev. B* **83**, 085426 (2011).
- [11] A. M. Essin and V. Gurarie, *Phys. Rev. B* **84**, 125132 (2011).
- [12] A. Blason and M. Fabrizio, *Phys. Rev. B* **108**, 125115 (2023).
- [13] N. Wagner, L. Crippa, A. Amaricci, P. Hansmann, M. Klett, E. J. König, T. Schäfer, D. D. Sante, J. Cano, A. J. Millis, A. Georges, and G. Sangiovanni, *Nature Communications* **14**, 7531 (2023).
- [14] Y.-Y. He, H.-Q. Wu, Z. Y. Meng, and Z.-Y. Lu, *Phys. Rev. B* **93**, 195164 (2016).
- [15] J. Zhao, P. Mai, B. Bradlyn, and P. Phillips, *Phys. Rev. Lett.* **131**, 106601 (2023).
- [16] M. Fabrizio, *Phys. Rev. Lett.* **130**, 156702 (2023).
- [17] A. Georges, G. Kotliar, W. Krauth, and M. J. Rozenberg, *Rev. Mod. Phys.* **68**, 13 (1996).
- [18] T. Maier, M. Jarrell, T. Pruschke, and M. H. Hettler, *Rev. Mod. Phys.* **77**, 1027 (2005).
- [19] O. Parcollet, M. Ferrero, T. Ayrál, H. Hafermann, I. Krivenko, L. Messio, and P. Seth, *Computer Physics Communications* **196**, 398 (2015).
- [20] P. Werner, A. Comanac, L. de' Medici, M. Troyer, and A. J. Millis, *Phys. Rev. Lett.* **97**, 076405 (2006).
- [21] E. Gull, A. J. Millis, A. I. Lichtenstein, A. N. Rubtsov, M. Troyer, and P. Werner, *Rev. Mod. Phys.* **83**, 349 (2011).
- [22] T. Stanescu, M. Civelli, K. Haule, and G. Kotliar, *Annals of Physics* **321**, 1682 (2006).
- [23] M. Ferrero, P. S. Cornaglia, L. De Leo, O. Parcollet, G. Kotliar, and A. Georges, *Phys. Rev. B* **80**, 064501 (2009).
- [24] L. Crippa, A. Amaricci, S. Adler, G. Sangiovanni, and M. Capone, *Phys. Rev. B* **104**, 235117 (2021).
- [25] In the OBC geometry we used the fit parameters of the results in PBC to construct the hopping processes in $H_0(\mathbf{k})$ and $H_1(\mathbf{k})$. Starting from that we construct the matrices of $H_0(\mathbf{k})$ and $H_1(\mathbf{k})$ with PBC along x and OBC with $N_y = 200$ layers along y.
- [26] A. Blason, I. Pasqua, M. Ferrero, and M. Fabrizio <https://doi.org/10.48550/arXiv.2406.15143>.
- [27] M. Fabrizio [10.1038/s41467-022-29190-y](https://doi.org/10.1038/s41467-022-29190-y) (2022).
- [28] We acknowledge Gabi Kotliar for this observation, closely related to the conclusion of his work [31].
- [29] N. Wagner, D. Guerci, A. J. Millis, and G. Sangiovanni, Edge zeros and boundary spinons in topological mott insulators (2023), [arXiv:2312.13226](https://arxiv.org/abs/2312.13226) [cond-mat.str-el].
- [30] T. A. Maier, M. Jarrell, T. C. Schulthess, P. R. C. Kent, and J. B. White, *Phys. Rev. Lett.* **95**, 237001 (2005).
- [31] M. Grilli and G. Kotliar, *Phys. Rev. Lett.* **64**, 1170 (1990).